MOTOROLA LABS

RF DOSIMETRY FOR THE FERRIS-WHEEL MOUSE EXPOSURE SYSTEM

Final Report, August 2, 2004

Antonio Faraone, Maurice Ballen, Giorgi Bit-Babik, Andrew V. Gessner, Michael Y. Kanda,

Mays L. Swicord, and Chung-Kwang Chou

Corporate EME Research Laboratory, Motorola Labs, Fort Lauderdale, Florida, USA

Wilson Luengas, Subbarao Chebrolu, Tadeusz Babij

Florida International University, Electrical and Computer Engineering Department,

Miami, Florida, USA

Contact: Antonio Faraone, Ph.D.

Motorola Corporate EME Research Laboratory

8000 West Sunrise Boulevard

Fort Lauderdale, FL 33322, USA

Phone: +1-954-723-4413

Fax: +1-954-723-5611

E-mail: antonio.faraone@motorola.com

1

ABSTRACT

Numerical and experimental methods were employed to assess the individual and collective dosimetry of mice in Ferris-Wheel exposure systems used in a lifetime bioassay on 1200 mice exposed to pulsed RF energy at 900 MHz (Utteridge *et al.*, *Radiat. Res.* **158**, 357-364, 2002). Twin-well calorimetry was employed to measure the whole-body SAR of mice for three body masses (23 g, 32 g and 36 g) to determine the lifetime exposure history of the mice employed in the bioassay. Calorimetric measurements showed about 95% exposure efficiency, and lifetime averaged whole-body SAR levels of 0.21, 0.86, 1.7, and 3.4 W kg^{-1} for the four different exposure groups. The largest statistical SAR variation was observed in the smallest mice, due to larger posture variation inside the plastic restrainers. Infrared thermography provided SAR distributions over the sagittal plane of mouse cadavers. Thermograms typically showed SAR peaks in the abdomen, the neck, and the head. The peak local SAR at these locations, determined by thermometric measurements, showed peak-to-average SAR ratios below 6:1, with typical values around 3:1. Results indicate that the Ferris-Wheel fulfills the requirement of providing a robust exposure setup for mice with uniform collective lifetime exposure.

INTRODUCTION

The Ferris-Wheel exposure system was designed to enable a large-scale bioassay (*1*) conducted at the Institute of Medical and Veterinary Science (IMVS) in Adelaide, South Australia, that was a follow-up to an earlier bioassay conducted on transgenic Eμ-Pim1 mice by Repacholi *et al.* (*2*). It was also employed by Finnie *et al.* in studies on the vascular permeability in mouse brain (*3-4*). The features of the Ferris-Wheel exposure system have been reported in an earlier publication by Balzano *et al.* (*5*). Fifteen systems were installed at IMVS in March 1999 and the two-year follow-up bioassay was carried out between mid-1999 and mid-2001 by Utteridge *et al.* (*1,6*), using 1200 exposed mice (including 240 sham controls) plus 400 cage control mice. The results indicated no change in tumor incidence in wild type and transgenic mice exposed for two years at five levels of dose rates. The follow-up nature of this bioassay required that a large mouse population be employed and possible dose-response effects be investigated, targeting five *whole-body average* (WBA) *specific absorption rate* (SAR) levels: 0 (sham), 0.25, 1, 2, and 4 W kg^{-1}. The exposure design goal was to control the WBA-SAR to within ± 2 dB over the long exposure period, under the assumption that the mean weight of adult mice would reach 30 g. To achieve as uniform as possible a collective lifetime exposure, the location of mice was randomly rotated in the exposure system on a daily basis, thus the nickname "Ferris-Wheel."

This paper reports the results of a detailed dosimetric characterization of the Ferris-Wheel exposure system, so as to complement the results of the follow-up bioassay. As shown by the authors' affiliations, the dosimetric study was conducted at the Motorola Corporate EME Research Laboratory in Fort Lauderdale, Florida, in collaboration with the Florida International University, Miami, Florida, following well-established techniques developed in the field of RF dosimetry (*7–8*). Materials and methods employed in this study are described while illustrating the various techniques

employed to carry out a preliminary analysis using dummy loads, prior to achieving the definitive

and complete dosimetry characterization using mouse cadavers.
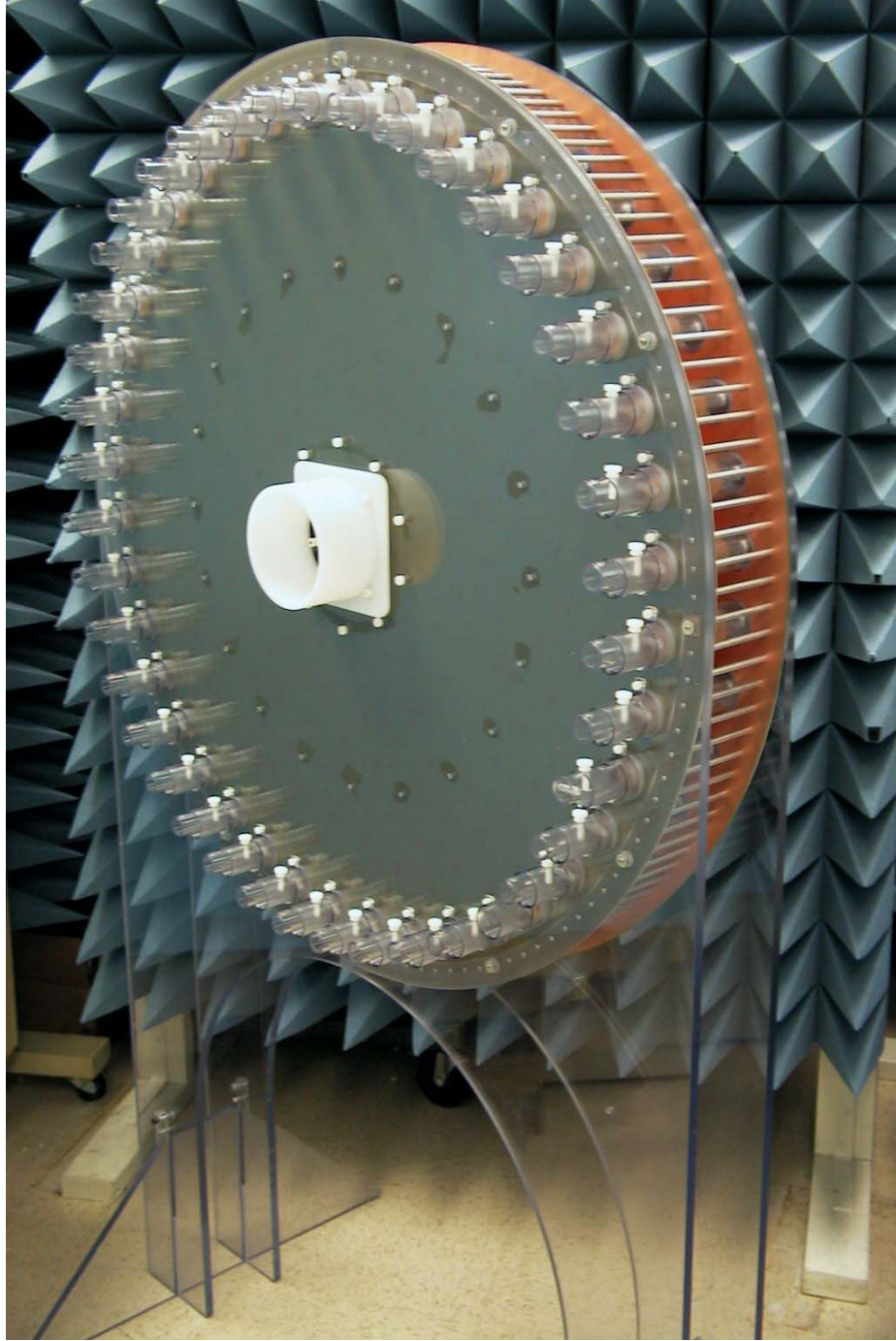
Fig. 1. Photograph of the Ferris-Wheel exposure system employed in the dosimetric study.

MATERIALS AND METHODS

The Ferris-Wheel exposure system, shown in Figure 1, is a radial cavity where an electromagnetic field is excited by means of a tunable feeder placed at the geometrical center (*5*). It holds forty mice that are restrained in plastic tubes so the long axis of their body remains co-polarized with the incident E-field. The system employed in the present study was essentially identical to the fifteen systems used at IMVS, which allowed the simultaneous exposure of 600 mice, and daily exposure of 1200 mice divided into morning and afternoon shifts (transgenic and regular mice). Because live mice were not employed in this dosimetry study, the external air-supply system was removed. A high input power level (up to 350 W *rms*) was required, which ran a risk of damaging the exposure system feeder. Thus four small holes (1 cm diameter) were drilled in the Teflon cylinder that holds the circular plates together to allow visual inspection of the feeder integrity. An 8-channel RF generator with an 8-way power combiner (Model 1020, Cheung Laboratories, Columbia, MD) was used to energize the exposure system. The generator operates in the 915 MHz ISM band, a slightly higher frequency than the one used at IMVS (898.4 MHz). We determined that such a small difference (about 2%) was acceptable for reproducing the exposure conditions experienced by the mice. Forward and reflected power were monitored using a bi-directional coupler (Model 3020A, Narda, Hauppauge, NY) and power meters (Model E4418B, HP/Agilent, Palo Alto, CA), connected after the combiner, before a 50-cm long, 1.59 cm (5/8") diameter coaxial cable running to the cavity feeder. The setup was capable of producing RF power in excess of 400 W *rms* but was typically set between 300 W and 350 W. A photograph and block diagram of the RF power generation setup are provided in Figure 2. Power meter readings were collected during each experiment. The net input power at the Ferris-Wheel feed point was

determined by taking into account the insertion loss of the coupler ($L_{CPL} \simeq 0.15$ dB) and the cable ($L_{CBL} \simeq 0.20$ dB). The following relation was used to determine the net input power[1] from the measurement of the forward (W_{fwd}) and reverse (W_{rev}) power at the coupler ports:

$$W_{net} = \gamma_{fwd} \cdot W_{fwd} - \gamma_{rev} \cdot W_{rev} \text{ , where } \gamma_{fwd} = 10^{-(L_{CPL}+L_{CBL})/10} \text{ , } \gamma_{rev} = 10^{L_{CBL}/10} \text{ . (1)}$$

Mouse cadavers of selected mass ranges for use in this dosimetric study were purchased from the Goodwin Institute for Cancer Research in Plantation, Florida.

Fig. 2. RF power generation and monitoring setup.

Techniques employed to determine the whole-body SAR average in exposed mice

We employed a differential, twin-well calorimeter technique to determine the WBA-SAR and

---

[1] The net power into each exposure system at IMVS was monitored by means of dual directional power sensors (Model Thruline 4525, Bird Electronic Corp., Cleveland, OH) yielding DC voltages proportional to the directional

analyze the uniformity of exposure versus position in the wheel (animal holder location) and body

mass. The twin-well calorimeter allows differential heat measurements between samples (exposed

and sham) of very similar mass. The difference in the heat exchanged with the constant temperature

envelope of the calorimeter was determined by measuring and integrating over time the output

voltage, which is produced by a thermocouple pile yielding the instantaneous temperature difference

between wells, by means of a digital multi-meter (Model 8540A, HP/Agilent) connected to a

personal computer via a General Purpose Interface Bus (GPIB). The calorimeter used in this study

was previously described by Chou *et al.* (*9-10*). The calorimeter envelope was kept at a constant

temperature by means of a circulating water bath (Model RC6 CS, Lauda Dr R Wobser GMBH,

Lauda-Konigshofen, Germany), as shown in Figure 3. The water bath would also control the

envelope temperature in a larger twin-well calorimeter that was used to stabilize the temperature of

the samples prior to the experiments as described in Chou *et al.* (*11*). We calibrated the instrument

using four different methods – involving ice, ice and water, or different water quantities in each well

– that proved to be equivalent to each other. The calorimeter calibration, featuring known thermal

loads and minimal operator interference, was also employed to establish the intrinsic uncertainty of

the calorimetric technique (~5%). As described in (*9*), the exponential decay constant for the

calorimeter response was determined once and for all so that data acquisition could be stopped after

about 20 minutes and the tail of the response could be extrapolated analytically. This resulted in a

significant increase in the daily number of exposures that could be conducted (up to ten in a day).

For the preliminary evaluations involving dummy loads, we employed the same plastic flasks

described in (*5*) (Model 05-529-1C, Fisher Scientific, Pittsburgh, PA) filled with 30-cc of tissue

simulating liquid ($\varepsilon_r = 51, \sigma = 1.0$ S m^{-1} at 900 MHz). The specific gravity of this liquid (~1.25 g

---

power flow. The low-pass cutoff of the power sensors was below the GSM frame rate, so a constant DC voltage was

cm^{-3}) was substantially higher than that of most actual biological tissues. SAR values were adjusted

accordingly.
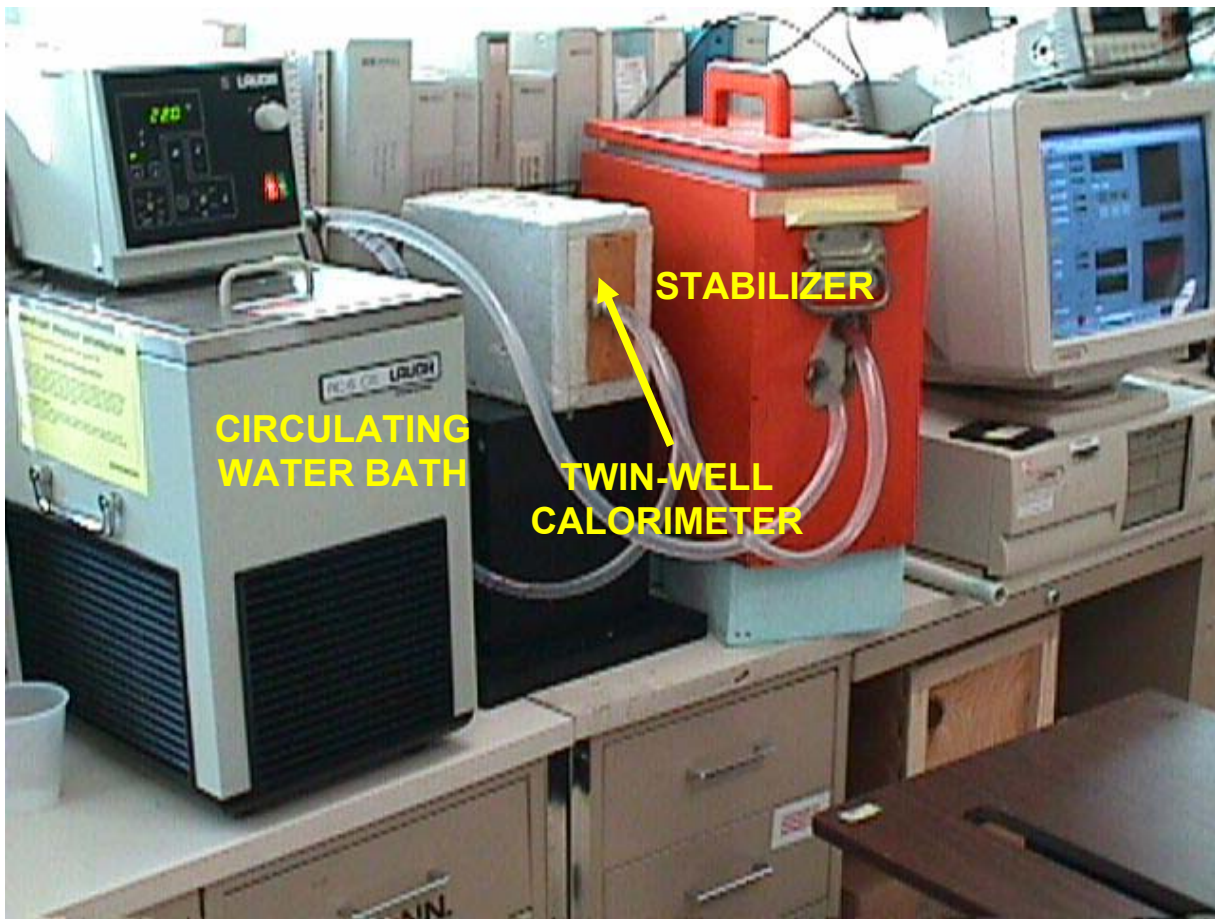
Fig. 3. Twin-well calorimeter setup for whole-body SAR measurements.

Each exposure required loading the Ferris-Wheel with 40 mouse cadavers. The same set of mice

could be used for only one day before excessive tissue decomposition. We performed the study

using three different mass groups (23, 32, and 36 g) in order to determine the SAR variability

experienced by the mice in the IMVS bioassay (*1*). Four locations on the wheel were assessed for

each mass group, each requiring typically ten runs (carried out over several days) in order to achieve

---

produced. The sensors nonlinear DC voltage response versus power was compensated for.

sufficient confidence in the mean of the resulting data distribution. At the end, the total number of mouse cadavers needed for calorimetry alone exceeded one thousand. In each experiment, all mice populating the wheel were selected to be within ± 1 g from the target mass for that group, thus ensuring that the exposed mouse was representative of the whole group. Mice of very similar mass were paired so as to be used as the exposed and sham-exposed samples. The mouse cadavers were kept frozen at –56°C. The night before or early on the day when experiments were conducted, forty-one mice of the selected mass group to be used for testing were thawed and allowed to equilibrate to room temperature (~23°C). Two (one exposed and one control) of them were used for the calorimetry test. We elected to use room temperature as the baseline temperature for these dosimetric studies. Operating at a temperature closer to the live mouse body temperature (38°C) would provide dielectric properties more closely aligned with living tissues. However, elevating the temperature of the mice under test would have created an artificial load asymmetry in the wheel because of the different dielectric properties between the exposed mouse under test and the other 39 mouse cadavers loading the Ferris-Wheel. Elevating the temperature of all the mice in the wheel would have been an extremely difficult proposition, if not impossible, and would have shortened their usability to no more than a few hours due to accelerated tissue decomposition. As a consequence, we would have had to use several times as many mouse cadavers, or conversely give up the accuracy attainable with a large number of exposure repetitions. Considering that it had been previously observed – during preliminary trials at IMVS after installation – that using live mice or mouse cadavers did not affect significantly the cavity impedance response, we opted for the more practical and repeatable test condition.

Immediately before exposure, one mouse cadaver was placed in the wheel while the other was placed in a "sham" restrainer identical to those employed in the Ferris-Wheel, which was mounted

on a wooden table. Two operators were needed to handle simultaneously the mice. To average out any operator bias, they swapped roles frequently. Experiments were run typically at 280-300 W net input power, corresponding to a whole-body SAR in the range of 200-320 W kg^{-1} depending on the collective mass of the mice (about 0.92 to 1.45 kg), for 30 s in order to induce an average whole-body temperature increase between 1.5°C and 3°C. Immediately after exposure, both mice were simultaneously transferred to the calorimeter (see Fig. 4). This delicate operation required careful handling to avoid heat exchange with the operators' hands and with the environment. To this purpose, the mouse cadavers were tied to a thin nylon string prior to the exposure. After exposure, they were pulled out of their restrainers by the string and placed in the calorimeter. The calorimeter lid was shut immediately and the output voltage was collected at a 2 s sampling interval through a computer connected to the digital multi-meter.

Fig. 4. Twin-well calorimeter loaded with exposed and sham-exposed 23-gram mice.

Besides characterizing the uniformity of exposure across different mouse locations in the wheel, calorimetric measurements also yielded two interrelated quantities, namely the exposure system efficiency and the normalized SAR. The former is defined as the ratio between the total power absorbed by the mice and the net input power, while the latter is the SAR per net input power (in units of W kg^{-1} W^{-1}). Power is dissipated in the mice, in the metals and dielectrics forming the cavity, or leaked to radiation. The RF energy absorbed in the mice and converted to heat is determined by comparing the difference in heat content between exposed and sham-exposed mice by means of the twin-well calorimeter. Some of the heat absorbed by the exposed mouse never reaches the calorimeter because it is released during exposure and during the transfer into the calorimeter. We have attempted to determine and correct for the latter, accepting the former as a small, uncompensated bias in our evaluation. Due to the thermal isolation provided by the mouse fur, which reduces heat loss during exposure and transfer, compensation was required when measuring dummy loads but not for mouse cadavers, except for the 23-g mice (probably due to their larger surface-to-volume ratio).

The preliminary efficiency estimates carried out in (*5*) indicated that efficiency greater than 90% was achievable. A detailed explanation of the method to determine efficiency and normalized SAR follows. The twin-well calorimeter yields a *dc* voltage reading that is proportional to the instantaneous temperature difference between the wells containing the sham and the exposed mice. By integrating the voltage over time, and using the calorimeter's conversion coefficient and any heat-loss compensation factor, we can estimate the excess heat ΔQ_{meas} induced by RF energy in the exposed mouse. Therefore, the average time-rate of RF energy dissipation in the exposed mouse is

$$W_{meas} = \frac{\Delta Q_{meas}}{\Delta t} \quad [W] \, , \qquad\qquad (2)$$

where Δt is the exposure duration (always about 30 s). The *exposure efficiency* for a sample placed in one particular location on the wheel is defined as the ratio between the absorbed power and what would be absorbed if the net power were equally distributed among all the mice in the wheel:

$$\eta = \frac{W_{meas}}{W_{net}/40} = \frac{W_{meas}}{W_{net}} \cdot 40 \ . \qquad (3)$$

Then, from the mass (m_{sample}) of the exposed group, the normalized SAR is found as follows

$$\overline{SAR} = \frac{SAR_{whole-body}}{W_{net}} = \frac{W_{meas}/m_{sample}}{W_{net}} = \frac{\eta}{40 \cdot m_{sample}} \quad \left(W \ kg^{-1} \ W^{-1}\right) . \qquad (4)$$

Once the efficiency and normalized SAR have been determined at N different locations, the *mean* efficiency and normalized SAR can be estimated as the corresponding averages. Ideally, one should perform the assessment at each location around the wheel (N = 40). However, time and resource constraints limited our ability to conduct such an extensive investigation. The results shown later are based on measurements of dummy loads or mouse cadavers at four different locations on the Ferris-Wheel (N = 4), namely *top*, *bottom*, *left*, and *right*. Depending on the variance of the measured data, five to fifteen runs were required for each location and mass to achieve 95% confidence interval bounds within 10% of the mean ($SE \le 5.1$).

Techniques employed to determine the SAR distribution in the exposed mice

Several different techniques were employed to assess the level and uniformity of SAR within the exposed mice. E-field probes were employed to carry out preliminary assessments of the SAR distribution in dummy loads. Infrared (IR) thermographic images of the SAR distribution over the sagittal plane of mouse cadavers were used to determine the highest SAR spots, where "RF-transparent" thermometers were subsequently placed to determine the local SAR and quantify the

degree of homogeneity of the SAR distribution.

Fig. 5. SAR measurements along the dummy load centerline by means of a miniature E-field probe.
The sketch illustrates geometry and dimensions of the dummy loads.

SAR measurements using E-field probe. A robotics system (Model DASY3, SPEAG AG, Zurich, Switzerland) was employed to operate a miniature E-field probe to sample the SAR along the centerline of the dummy loads. The experimental setup, shown in Figure 5, features the Ferris-Wheel laying horizontally, loaded with forty dummy loads. A miniature single-channel E-field probe (Model T1V2, SPEAG AG), featuring a 1-mm dipole with diode-detector, was operated by the robot in order to measure three orthogonal polarizations by rotating twice upon its axis by 120° at several locations along the dummy centerline. Additional liquid simulant was supplied with a syringe as the probe was extracted to maintain a constant liquid level in the load. These measurements provided the SAR distribution along the load centerline while also yielding a preliminary estimate of the exposure

uniformity around the wheel. Considering that E-field measurements were employed for relative

SAR comparisons only, the relevant measurement uncertainty components produce ~6% combined

uncertainty.

Fig. 6. Mouse cadavers tied to Styrofoam slab holders before foaming.

SAR measurements using IR imaging. The principles of thermographic dosimetry are well

explained by Guy (*12*). Thermographic measurements in this study involved a complex preliminary

procedure to perform the sagittal cut of mouse cadavers. A cylindrical cardboard molding with an

inner radius equal to that of the Ferris-Wheel plastic restrainers was fabricated in order to allow

casting of the mouse. The casting material was Polyurethane foam produced by two liquid

precursors, one being the catalyst. The mouse was first thawed and then tied to a thin Styrofoam

support using thin nylon strings, as shown in Figure 6. The mouse was then inserted into the

cylindrical molding and secured to assure that its body remained centered in the cylinder cross-section during the highly dynamic foaming process. The Polyurethane precursors were poured into the mold to form foam around the mouse. Thirty minutes after the foam settled, the cast was removed from the mold and was cut so as to fit exactly in the Ferris-Wheel plastic restrainer. The encapsulated mouse assembly was marked to identify the weight of the mouse, the sagittal cut-plane and other alignment features, and then frozen. The sagittal cut was performed on the frozen assembly (see Fig. 7) using a thin saw-tooth blade, and then the two halves of the mouse were tightly covered with polyvinyl screen film to avoid body fluid loss once the mouse thawed. In addition, the polyvinyl film prevented evaporation, thereby ensuring that the mouse body was isothermal before exposure. The film also interrupted conduction currents during exposure, thus only the top and bottom locations on the wheel were used for exposures to minimize the perturbation on the current distribution and the resulting SAR.

A few minutes before starting the exposure, liquid nitrogen was poured inside the IR camera (Model 9000, UTI, Sunnyvale, CA) to provide the cold temperature reference. A baseline thermographic image of one side of the bisected mouse was taken. The two halves were then rejoined and placed at the designated location in the wheel. Toothpicks were inserted in the foam for easier handling and to avoid heat exchange with the operator's hands. Immediately after a 30 s exposure at about 280 W net input power, the assembly was rapidly yet carefully removed from the Ferris-Wheel, the halves were separated, and the side whose baseline thermogram had been previously taken was placed once again in front of the camera and a second thermographic image was taken. A custom-shape Styrofoam stand, painted black matte, was fabricated to allow fast and repeatable positioning of the sample in front of the camera, a critical step to ensure accurate comparison of the "before" and "after" sagittal plane thermograms. The image acquisition to a PC

via GPIB and the subsequent processing was automatically performed by a custom software. Figure 8 shows an example of the raw data output and the processed plots.
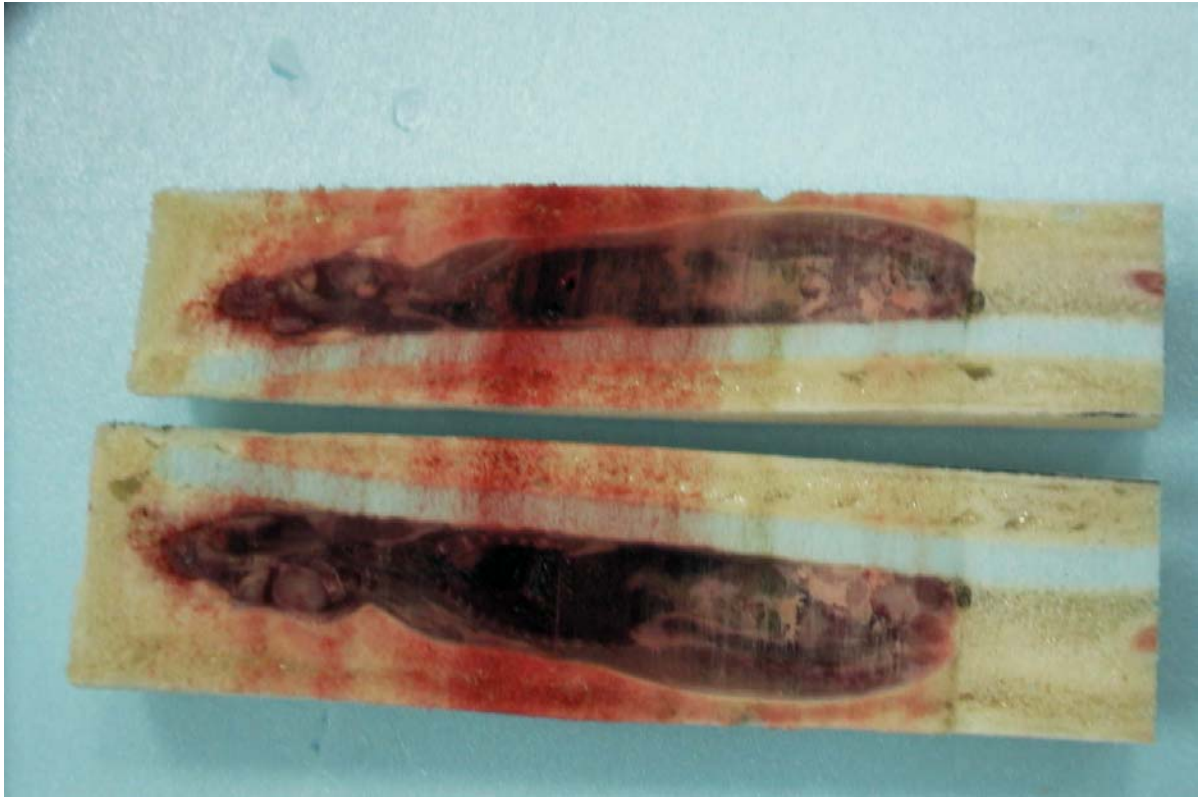
Fig. 7. Frozen mouse cadaver after sagittal plane cut. Bloodstains were removed before covering both halves with polyvinyl film.

SAR measurements using temperature sensors. Thermometry was used to determine the local SAR in areas of the sagittal plane where thermographic images showed exposure peaks consistently. We employed RF-transparent temperature probes of two kinds: *fluoroptic thermometers* (Model 3000, Luxtron, Santa Clara, CA) and *thermistors* (custom made by BSD Medical, Salt Lake City, UT). Both exhibit a resolution of better than $0.1^{o}C$ (*13–15*). Data acquisition was automated through RS-232 and GPIB ports, respectively, and post processing carried out on a personal computer. The

acquisition software (Lab View v4.3, National Instruments, Austin, TX) allowed four simultaneous

thermometer readings. Three sensor heads were inserted into tissue just below the surface at selected

locations on the sagittal plane and secured to the foam with transparent tape before the two halves

were joined. To avoid artifacts due to sensor heating, particular care was taken to route the

thermistor probes through holes in the mouse restrainer so as to run orthogonal to the incident

electric field. A fourth one was placed ~3 cm deep in the rectum of another mouse cadaver in the

wheel in order to monitor the body temperature during and between exposures to provide means of

determining when the other 39 mouse cadavers had returned to room temperature before starting a

new exposure.

The localized SAR was determined by measuring the initial time-rate of temperature rise over a

30 s exposure period with about 280 W net input power. The SAR was then calculated as follows

$$SAR = c \left. \frac{\partial T}{\partial t} \right|_{t \to 0} , \qquad (5)$$

where *c* is the *effective* specific heat capacity of the mouse tissue. We used $c = 3446$ J kg^{-1} K^{-1},

which is the average between the values provided by Hart ([16]) and Durney *et al.* ([17]) (3444 J kg^{-1} K^{-1}

and 3448 J kg^{-1} K^{-1}, respectively). The intrinsic uncertainty of temperature based SAR estimates is

dominated by the component associated to the specific heat capacity, which is large (~16%) because

we employ the *effective* heat capacity in our assessments rather than distinguishing between tissues.[2]

Temperature measurements indicated that some heat diffusion would actually take place within

the mouse body over the exposure period (even though negligible heat loss from the body was

observed, as mentioned earlier). That is why the thermographic images, which report the

temperature differential over the whole exposure time, were not used to determine point-SAR, but

---

[2] The estimate of the uncertainty of the *effective* specific heat capacity was derived from the human data listed in
([18]), assuming that its dispersion would be similar for mouse tissues, albeit with different absolute values

rather to determine consistent patterns of RF energy deposition so as to select the thermometer

locations accordingly.
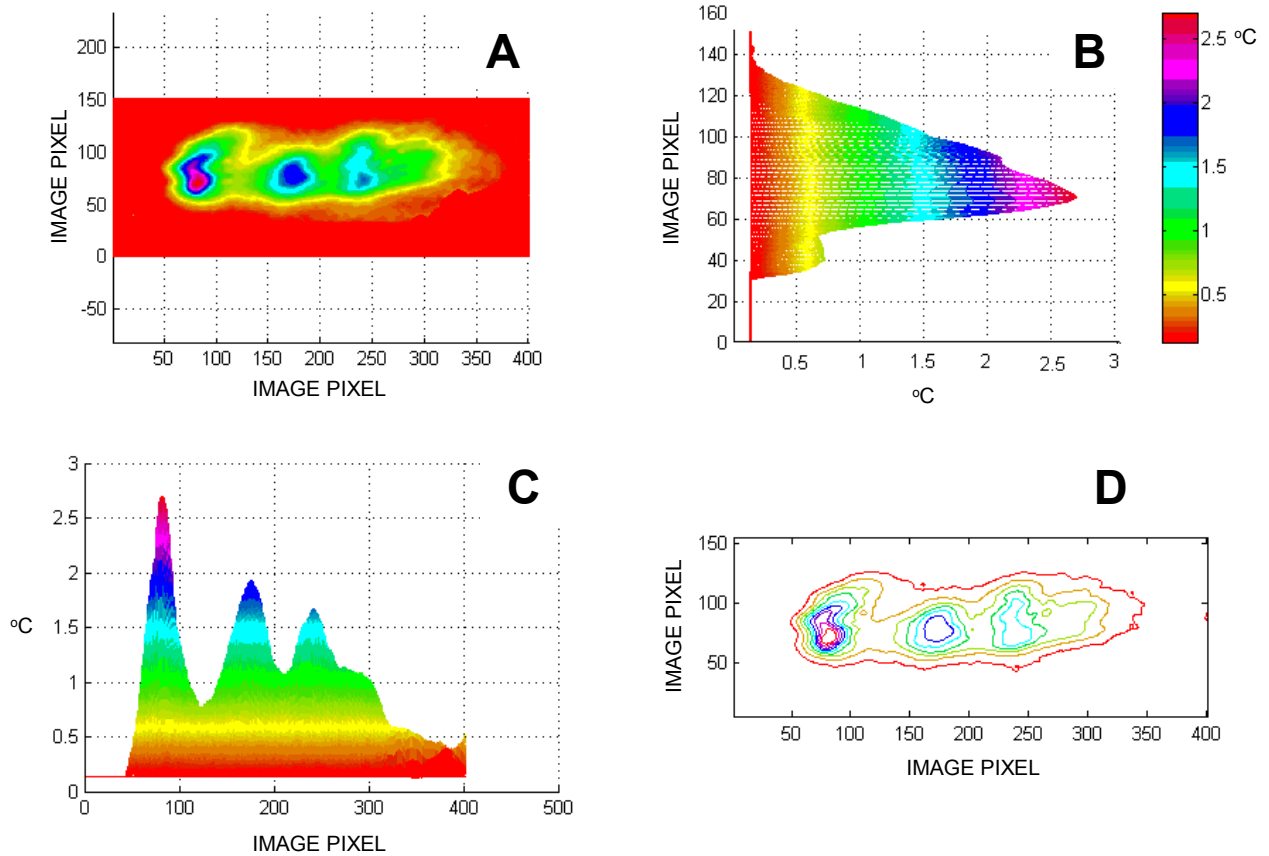
Fig. 8. Example of thermographic image post-processing featuring color level (A) and contour (D)

plots. Temperature distribution across the vertical image cut containing the peak surface temperature

(B). Temperature distribution across the corresponding horizontal image cut (C).

RESULTS

Computations and experiments aimed at establishing the soundness of the Ferris-Wheel design

are described first. Then we report the results concerning the WBA-SAR and the SAR distribution in

mouse cadavers. In the case of simulations, local SAR is averaged over a cubic volume enclosing

one gram of tissue in order to smooth out data roughness due to the discretized geometry. Point SAR

is shown in all other cases. Peak point SAR is always greater than peak 1-g SAR, but its estimate

may be less accurate. Measurement uncertainty is expressed in terms of the observed standard

deviations. Only in selected cases, the standard error (*SE*) or the peak-to-peak dynamic range are

employed and explicitly stated.

Computational assessment of the impact of asymmetries

A commercial simulation software (Microwave Studio, CST GmbH, Darmstadt, Germany) based

on the Finite Integration Technique (FIT) (*19*), was used to analyze the impact of asymmetries in the

Ferris-Wheel geometry or the load distribution on the whole-body and peak 1-g average SAR. The

complete computational model, shown in Figure 9, features 40 cylindrical loads with homogeneous

dielectric properties $\varepsilon_r = 51$, $\sigma = 1.0$ S m^{-1}, placed symmetrically around the wheel. Their axial

dimension (*h*) was kept at 60 mm while the radius (*a*) was varied in order to produce different mass

values (assuming 1000 kg m^{-3} specific gravity) so as to represent and actually exaggerate the mass

range experienced in the IMVS bioassay. Because of the large electrical size of the Ferris-Wheel

(about $2\lambda^3$, λ being the free-space wavelength at 900 MHz) and its round shape, the size of the

computational domain had to be in excess of $8\lambda^3$ to ensure accuracy of the Perfect Matching Layer

(PML) absorbing boundary conditions that allowed representing the spurious radiation process.

Moreover, given the small mesh size required by the high permittivity of the dummy loads, the total

number of volume elements (voxels) was extremely large, thus requiring prohibitively large memory

and computation times in excess of 10 hours.

MOTOROLA LABS
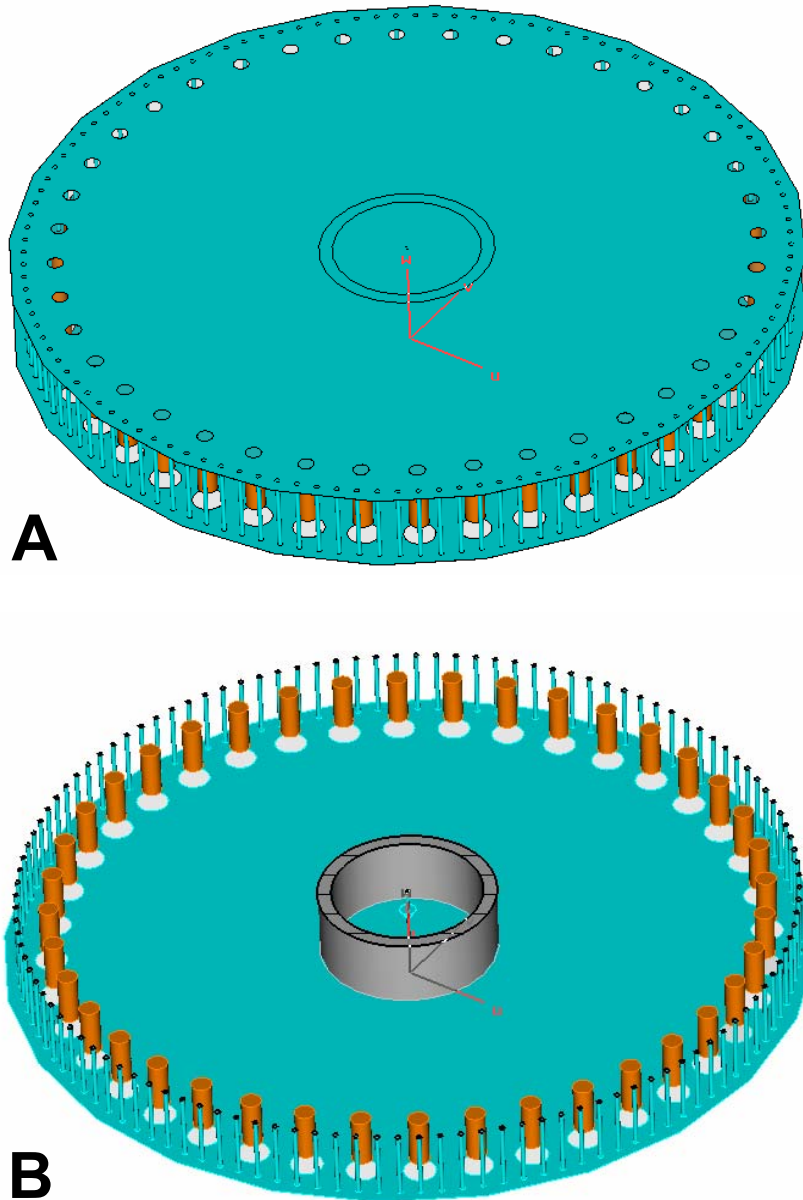
Fig. 9. Computational model of the Ferris-Wheel loaded with forty cylindrical dummy loads (A).

Exciter, Teflon ring support, holes for inserting the mice, and shorting bars are shown (B).

We introduced simplifications aimed at shrinking the electrical size of the Ferris-Wheel model, thus

reducing memory requirements and run time significantly. Since RF energy leakage from the Ferris-

Wheel is very low (less than 2% of the input power (*5*)), it is possible to neglect it in the model by

substituting the holes in the circular plates with Perfect Magnetic Conductor (PMC) surfaces, and

the array of shorting bars with a continuous, cylindrical Perfect Electric Conductor (PEC) wall (see

Fig. 10). The overall problem size was reduced to less than $3\lambda^3$, thus bringing run time down to

about 4 hours. To verify that the above-mentioned simplifications would not introduce artifacts, we

compared the model using PML and the one using PEC/PMC, loaded by equal weight dummies ($h =$

60 mm, $a = 12.5$ mm, i.e., 29.5 g). The results, for 1 W net input power, are summarized in Table 1.

TABLE 1
Impact of simulation model simplifications

Model	SAR_{WBA} (W kg^{-1})	SAR_{1-g} (W kg^{-1})	SAR_{1-g} / SAR_{WBA}
PML	0.41	0.98	2.38
PEC/PMC	0.42	0.99	2.39
% Difference	1.6%	1.3%	0.3%

Note: in both cases the net input power is 1 W.

The observed difference is 1.6 % between the whole-body averages and 1.3 % between the peak 1-g

averages. The ratios between peak 1-g and whole-body SAR averages differ only by 0.3 %,

indicating that the SAR distribution remained essentially unaltered.
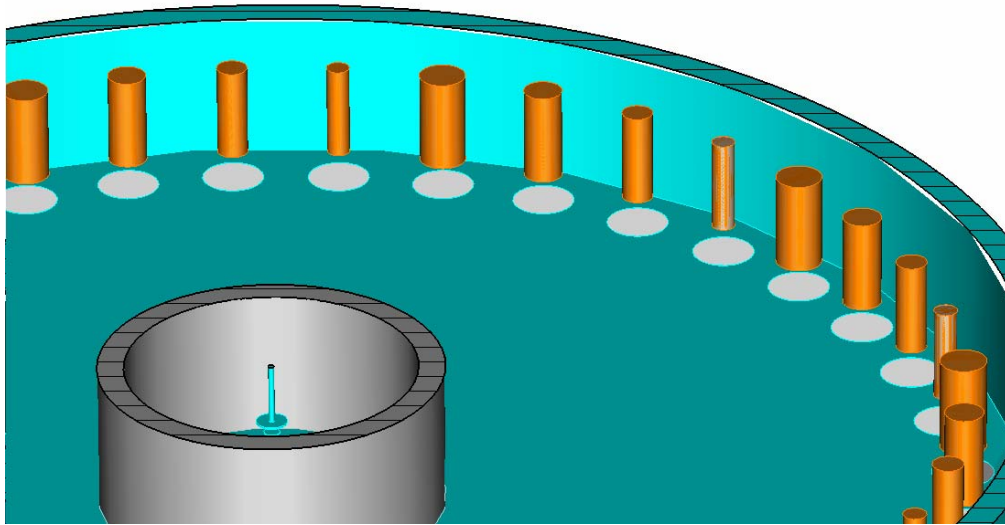
Fig. 10. Detail of the simplified Ferris-Wheel model loaded with dummy loads of four different

mass values, according to the sequence illustrated in Table 2 (Case #2).
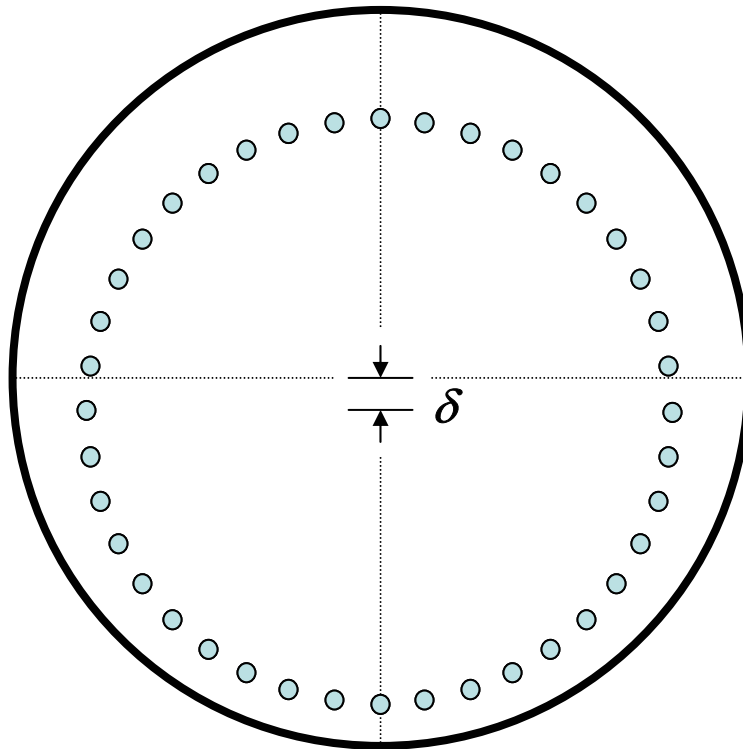
Fig. 11. Radial offset (δ) of the Ferris wheel loads with respect to the geometrical center.
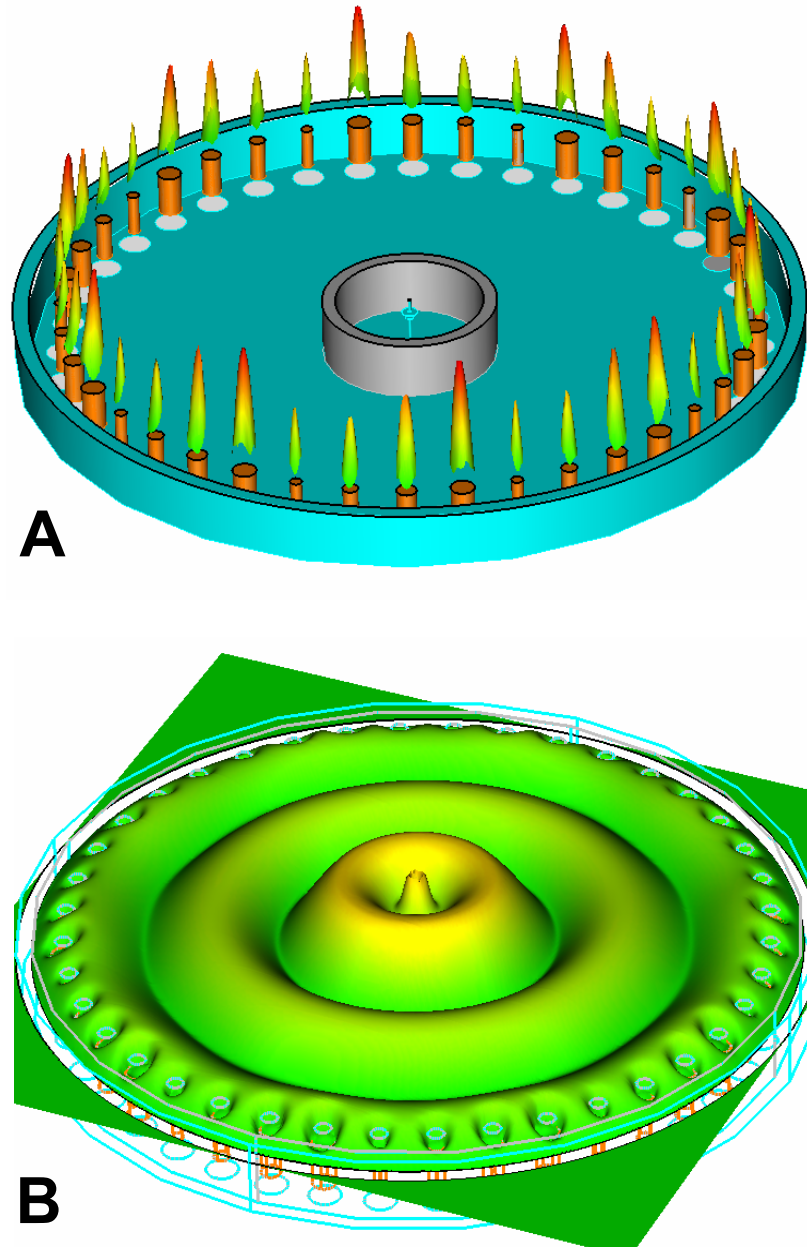
Fig. 12. Qualitative cross-sectional SAR distribution in the dummy loads for Case#2 (A) and corresponding distribution of the total electric field in the Ferris-Wheel (B).

We simulated cases of loads with different mass value, and cases of offset of the wheel load with respect to the Ferris-Wheel geometrical center. In the former instance, two cases were analyzed with two and four different mass values respectively. The corresponding results are reported in Table 2.

MOTOROLA LABS

TABLE 2

Impact of asymmetric mass loads. The mass sequences are repeated to load the Ferris-Wheel

a (mm)	Mass (g)	W_{abs} (mW)	SAR_{WBA} (W kg^{-1})	SAR_{1-g} (W kg^{-1})	SAR_{1-g} / SAR_{WBA}
Case #1: Two mass values					
10	18.8	12.3	0.65	1.29	1.98
15	42.4	36.5	0.86	2.17	2.51
Case #2: Four mass values					
7.5	10.6	9.3	0.88	1.28	1.45
10	18.8	13.4	0.71	1.40	1.98
12.5	29.5	24.7	0.84	2.02	2.40
15	42.4	47.9	1.13	2.83	2.51

Note: in all cases the dummy load height is $h = 60$ mm and the net input power is 1 W.

The computational model corresponding to the case with four different mass values is shown in Figure 10. Table 2 also reports the computed absorbed power (W_{abs}) by the loads, which sums up to about 97% and 95% of the net input power for Case #1 and Case #2, respectively. The latter instance (load offset) corresponds to using equal loads and shifting their collective center of mass away from the geometrical center of the Ferris-Wheel in a radial direction (as sketched in Fig. 11). The corresponding results are presented in Table 3.

TABLE 3

Impact of load offset asymmetry. Ratios between collective maximum and minimum SAR

δ (mm)	WBA	1-g	SAR_{1-g} / SAR_{WBA}
Case #3: Offset-type asymmetry			
0	1.0	1.0	2.38
2.5	2.6	2.4	2.39 ± 10 %
5	4.2	3.7	2.37 ± 11 %
10	24.9	20.4	2.36 ± 20 %

Note: in all cases $h = 60$ mm, $a = 12.5$ mm, and the net input power is 1 W.

Load-mass asymmetry. The variation in the normalized WBA-SAR is about ± 1 dB (0.89 W kg^{-1} W^{-1} ± 26 %) in Case #2 with four different masses (4:1 maximum mass ratio). The load variation for this extreme case is distributed circumferentially with spatial period of almost one wavelength, thereby enhancing the ability of the asymmetrically loaded wheel to induce higher-order circumferential modes. The corresponding variation in Case #1 is only about ± 0.6 dB. Due to stronger eddy currents, the larger loads exhibit larger peak 1-g to whole-body SAR ratio. It is interesting to notice that the ratios between peak 1-g and whole body SAR is quite insensitive to the asymmetry introduced in the model, showing how the SAR distribution within the load is negligibly affected by rather significant geometrical asymmetries in their neighborhood. In practice, we can expect that the nearby mice minimally affect the mechanism of energy absorption, which depends mainly on the mouse size. The total E-field plot in Figure 12, showing excellent azimuth symmetry in the presence of severe load asymmetry and correspondingly asymmetrical SAR distribution, further reinforces this notion.

Load-offset asymmetry. Identical loads ($h = 60$ mm, $a = 12.5$ mm, 29.5 g) were assumed and analyzed for three cases with offsets (δ) of 2.5, 5, and 10 mm, respectively. The results in Table 3, reporting the peak ratio between the collective maximum and minimum SAR (whole-body and 1-g SAR averages), indicate that this kind of asymmetry could introduce unacceptably high non-uniformity. The ratio between 1-g and WBA-SAR is still about 2.4 for the 29.5 gram loads, showing once again the relevance of the mouse size.

Finally, it is worth mentioning that the asymmetry introduced in the computational model by bending the feeder was responsible for severe effects similar to those produced by the load offset. For the sake of brevity, the corresponding results are omitted.
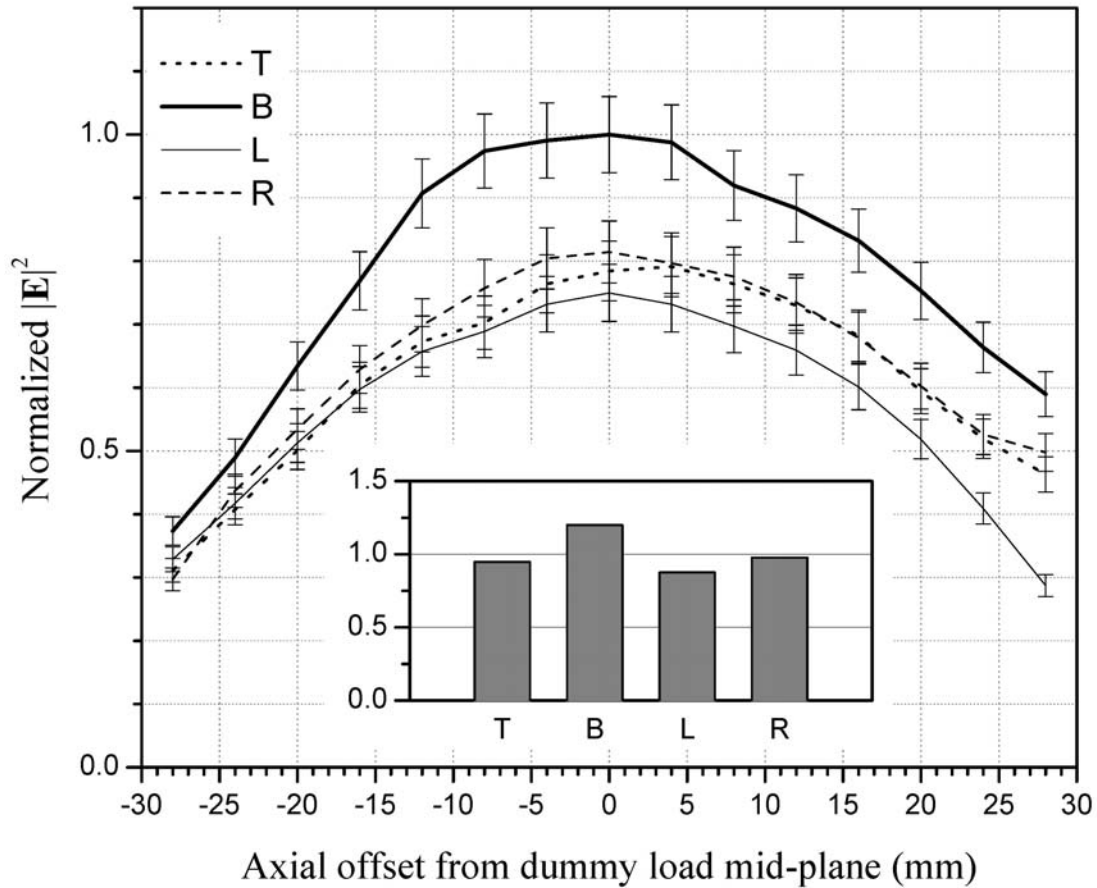
Fig. 13. Normalized E-field probe response along the dummy load centerline at four locations in the Ferris-Wheel. The inner chart compares the areas underneath the curves, which are proportional to the volumetric SAR averages in the dummy load, normalized to their collective average value.

Measurements on dummy loads

We employed the E-field measurement technique described earlier to obtain a preliminary indication of any serious effects due to possible asymmetries. The SAR along the load centerline was measured at the four locations within the Ferris-Wheel employed throughout the study: top (*T*), bottom (*B*), left (*L*), and right (*R*). The SAR profile, reported in Figure 13, follows the typical pattern produced by eddy currents, as pointed out in an earlier computational investigation by Russo and

Faraone (*20*). Three curves are closely grouped together, the fourth one (bottom position) being about 1 dB higher in the middle. The areas underneath the curves, which are proportional to the corresponding SAR averages over the volume of the dummy, differ within ± 0.7 dB, thus indicating no major asymmetry of the exposure.
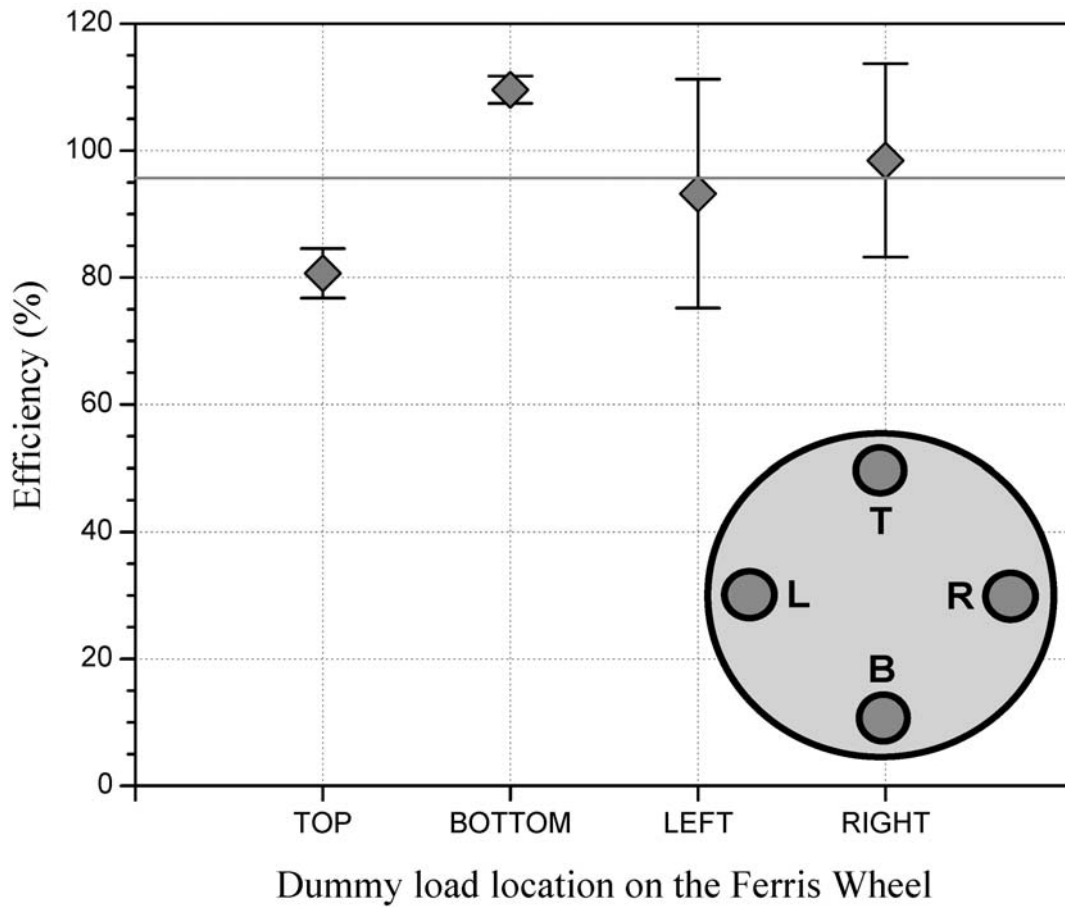
Fig. 14. Measured efficiency at four locations when the Ferris-Wheel is loaded with 40 dummy loads. A line indicates the average efficiency (95.5%).

The final assessment of exposure uniformity performed on dummy loads was carried out using differential twin-well calorimetry. Figure 14 reports the measured efficiency at four locations. Four

determinations were made for the top and bottom locations and six were made for the left and right

locations. The average efficiency estimate was 95.5% ±10%, almost equal to the 98% estimate in

(*5*). The measured variation was only ± 0.7 dB peak-to-peak, even though top and bottom locations

exhibited statistically different SAR values. Also, greater experimental uncertainty is noticeable at

the left and right locations. The corresponding average normalized SAR was 0.8 W kg^{-1} W^{-1}.

Whole-body average SAR in mouse cadavers

Three groups with a measured average mass of 23.2 ± 0.8 g, 31.9 ± 0.6 g, and 35.9 ± 0.4 g were

used. Inserting these values and the efficiency estimate just derived into Eq. 4, the expected

normalized SAR for each mouse group was 1.03 ± 0.10 W kg^{-1} W^{-1}, 0.75 ± 0.07 W kg^{-1} W^{-1}, 0.67 ±

0.07 W kg^{-1} W^{-1}, respectively. Table 4 summarizes the normalized SAR values for all combinations

of mass and location, together with the standard error (*SE*) and the number of exposures (N_{exp}).

TABLE 4
Normalized SAR (W kg^{-1} W^{-1}), associated percentile standard error and number of exposures

Mass Group	23 g			32 g			36 g		
Location	Mean	%SE	N_{exp}	Mean	%SE	N_{exp}	Mean	%SE	N_{exp}
Top	0.88	4.8%	11	0.80	3.9%	15	0.71	4.8%	6
Bottom	1.01	2.4%	10	0.78	3.3%	10	0.64	5.1%	8
Left	0.98	4.6%	9	0.80	2.5%	10	0.63	3.1%	12
Right	0.89	4.4%	5	0.76	2.6%	9	0.61	3.3%	8
Average	0.94			0.78			0.65		

In Figure 15, they are reported together with the standard deviation and compared with the expected

range of variation. The typical mouse WBA-SAR measurement uncertainty was ~11%, higher than

the ~5% intrinsic uncertainty of the calorimeter method. The difference is explained by the

additional sources of variations besides the calorimeter, including the mouse posture, the RF power

generation setup, and complex operator handling of the mouse cadavers. The 23-g data dispersion is the largest, probably due to larger posture variation of the smallest mice in the restraining tubes.
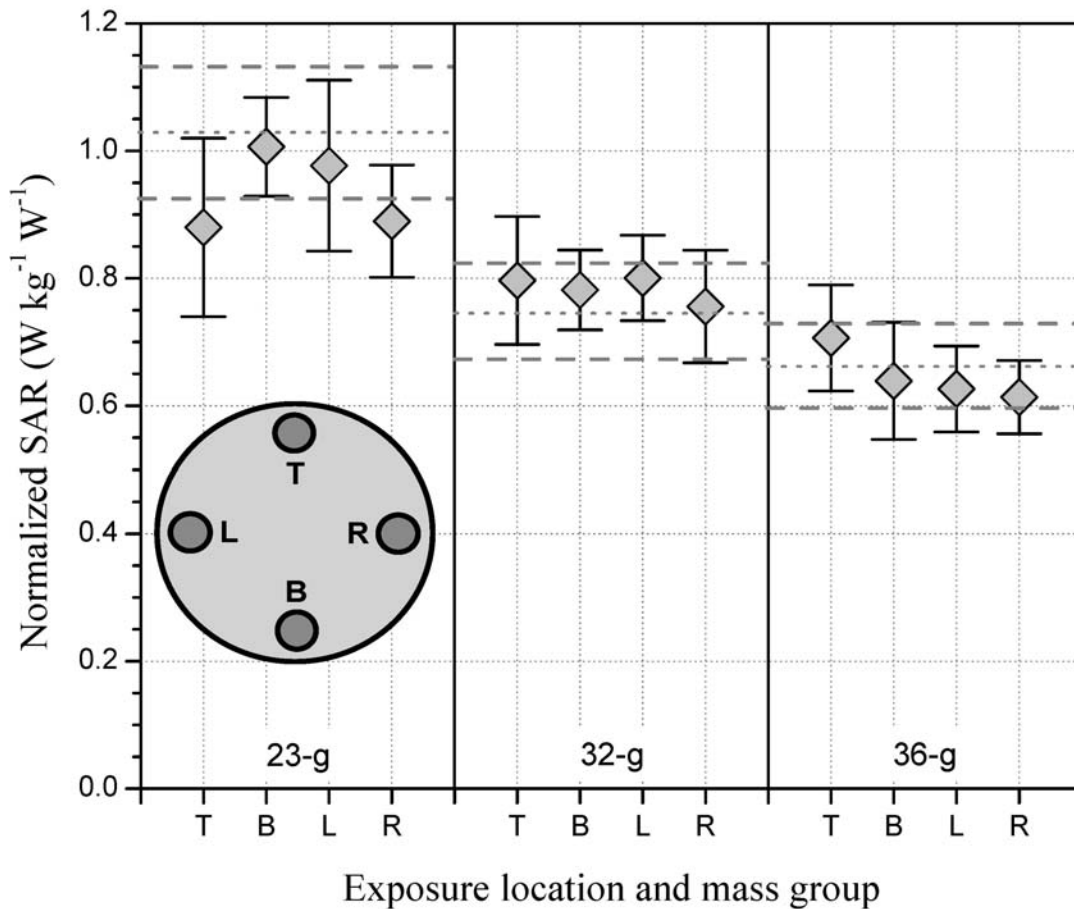
Fig. 15. Normalized WBA-SAR at four test locations with the wheel loaded with 40 mouse cadavers of three mass groups. Dotted lines indicate the range predicted using the 95.5% efficiency estimate.

Over the selected mass range and locations, the peak-to-peak normalized SAR variation is about ± 1.1 dB (29%). This variation accounts for different mouse locations on the wheel, so it is indicative of the overall swing in the lifetime exposure experienced by the mice at IMVS. The grand average of the whole data pool yields a normalized WBA-SAR of 0.79 W kg^{-1} W^{-1}. In particular, the

average normalized SAR is 0.94 W kg^{-1} W^{-1} for the 23-g mice, 0.78 W kg^{-1} W^{-1} for the 32-g mice, and 0.65 W kg^{-1} W^{-1} for the 36-g mice. The corresponding average efficiency estimates, obtained by inverting Eq. 4, are 87%, 99%, and 93%, all within ± 0.5 dB from the 95.5% average efficiency value established with the dummy loads, quite a good agreement considering the uncertainty and complexity of calorimetric techniques using animals. Only the estimate for the 23-g mice can be considered significantly different (0.4 dB lower). As mentioned earlier, one possible explanation is that some absorbed energy may have been lost *during* exposure due to higher body-average temperature rise and larger body surface-to-volume ratio, compared with the larger mass groups. We investigated another possible cause in the RF energy leakage, by measuring the radiation pattern of the Ferris-Wheel populated with 24±1 g versus 34±1 g mice, to determine whether it was higher for the former. Elevation pattern measurements, taken in the anechoic chamber at the Motorola facility in Plantation, Florida, using the same method employed in (*5*), indicated that the RF energy leakage is indeed slightly larger (4% compared to 2%) when the exposure system is loaded with smaller mice. We also discovered that the leakage is slightly higher if the mouse tails hang outside of the plastic restrainer, as if they behaved like antennas. However, the observed differences make up for only one-fourth of the ~8% missing efficiency.

SAR distribution in mouse cadavers

In this phase of the study we used many of the mouse cadavers that fell just outside of the strict mass specifications (± 1 g) adopted for the calorimetric study, thus making full use of the mouse cadavers available. Because they fell within three mass ranges (23-24 g, 26-28 g, and 33-36 g), they are labeled 24, 27, and 34 g for simplicity. The normalized WBA-SAR versus mass for these mice – used later on to determine peak-to-average SAR ratios– was determined by interpolating the results

obtained for the mass groups used for calorimetry. As shown in Figure 16, typical contour plots of IR thermograms of the sagittal plane of mice exposed in the Ferris-Wheel reveal three "hot spots." These are regions where higher temperature rise was consistently observed in the great majority of the experiments. They correspond to an area in the head, where highly conductive high-water content tissues are found; an area in the neck, due to high current density induced by the narrowing of the current path; and in the abdomen due to eddy currents. This qualitative information was used to select the locations where "RF-transparent" thermometers were placed to perform absolute measurements.
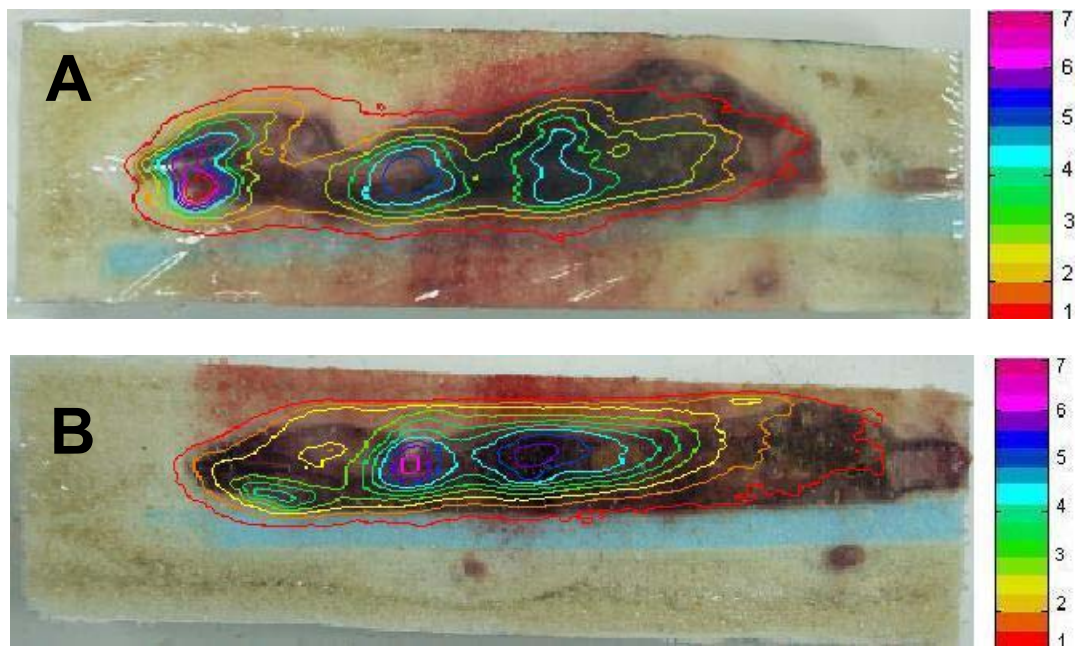

Fig. 16. Temperature distribution measured over the sagittal plane of 24-g mouse cadavers exposed at the top (A) and the bottom (B) locations on the Ferris-Wheel. Temperature isolines are superimposed on the photographs taken before exposure. The scale is in degree Celsius.
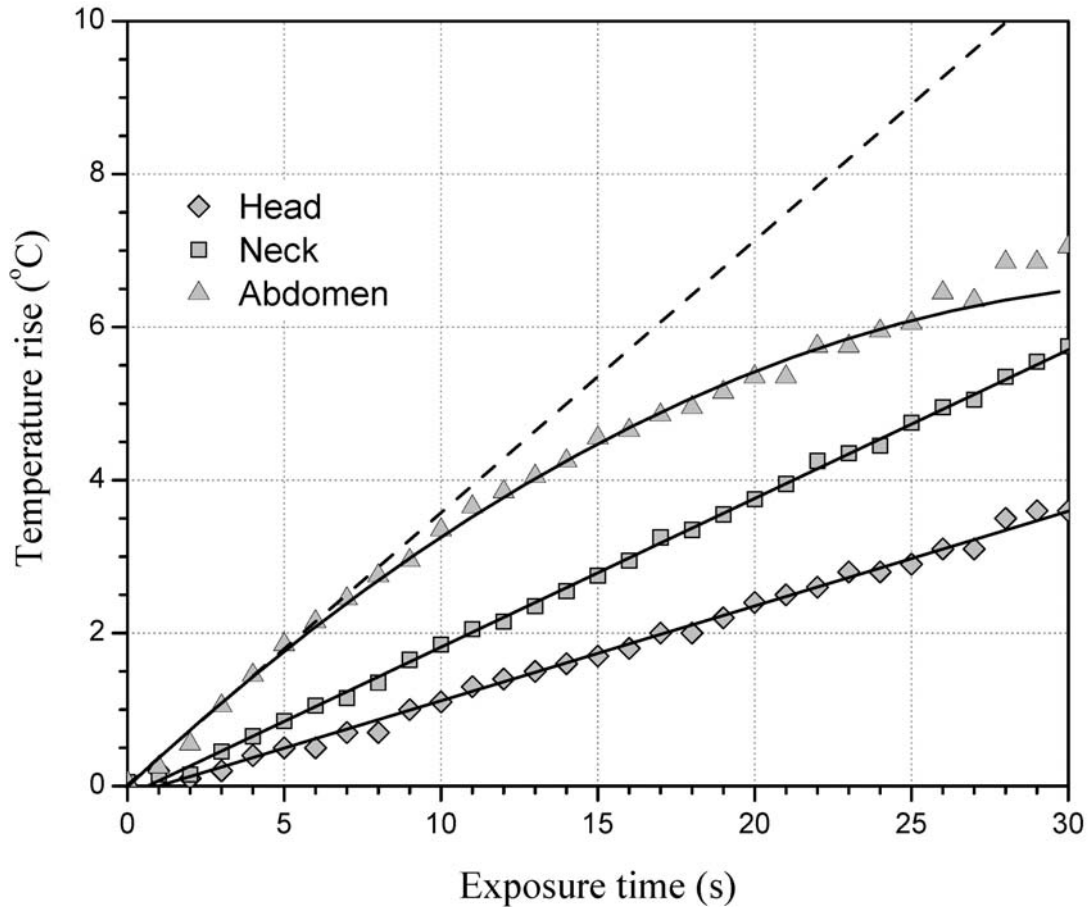
Fig. 17. Temperature measured at the three hot-spot locations over a 27.4 g mouse sagittal plane. The measured rise in the abdomen is fitted with a polynomial yielding the initial slope (dotted line).

An example of localized temperature measurement is provided in Figure 17. In this example, the highest temperature rise occurs in the abdomen. The heat diffusion becomes significant when high temperature rise occurs, as observed from the change in slope of the abdomen temperature after just a few seconds. The original initial slope was retrieved by polynomial interpolation of the measured behavior. The linear term of such an interpolation represents the initial slope that appears in Eq. 5. The temperature rise at the other two locations is substantially linear and does not require any special manipulation.
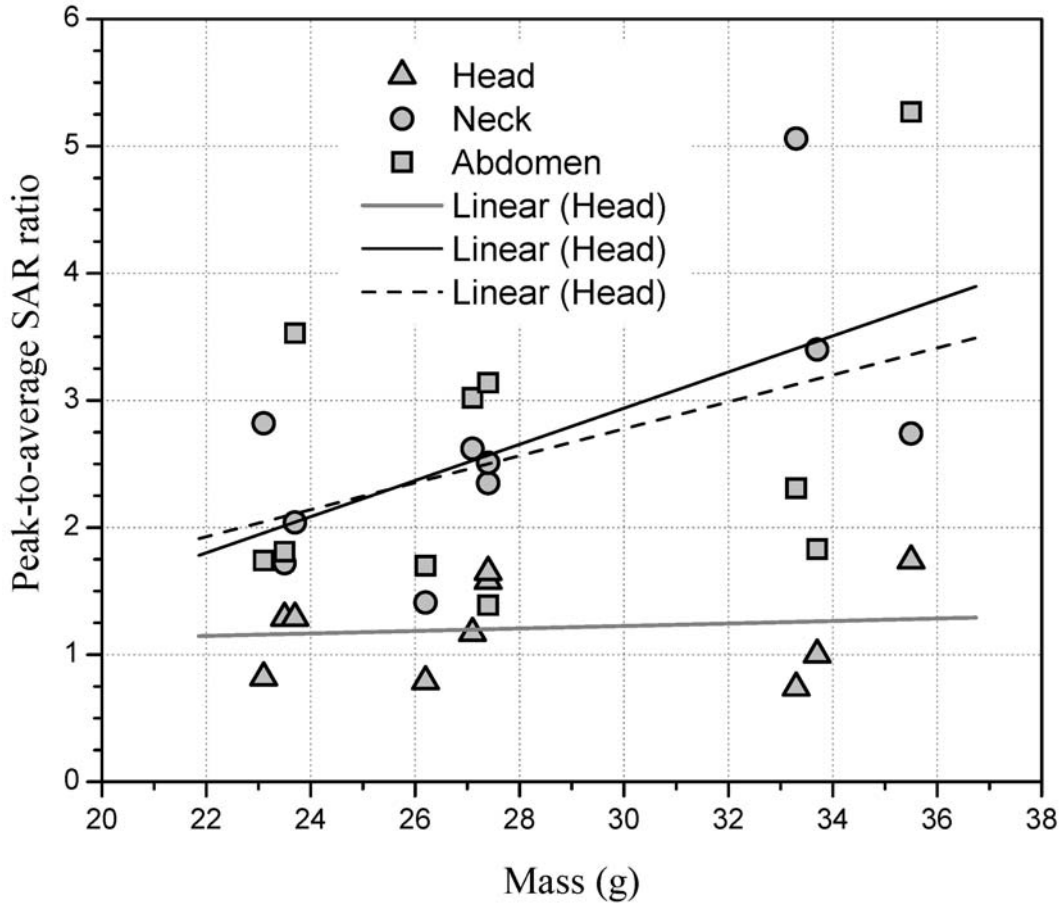
Fig. 18. Ratios between measured SAR at the head, neck, and abdomen and the whole-body SAR. Linear regression lines are shown for each location.

The results relative to the thermometric measurements are displayed in Figures 17 and 18. Figure 18 reports the peak-to-average SAR ratios measured at the hot-spots in the head, neck, and abdomen, of ten mouse cadavers (four at the bottom and six at the top locations in the wheel). The total number of valid exposures was 18 since two to three exposures per mouse were performed in most cases. The corresponding results were averaged for each mouse. The largest measured peak-to-average SAR ratio is less than 6:1, but in most cases the ratio is about 3:1. This result is consistent with the predictions of the simplified computational model describer earlier, which showed close to

a 2.5:1 ratio between the 1-g and the WBA-SAR. Interestingly, the regression lines follow a growing

trend versus mouse mass similar to that observed in the computations. A different breakdown of the

results, reported in Figure 19, shows that the SAR in the head is fairly independent from the mass

group, whereas higher ratios and stronger dependence are observed at the neck and abdomen. This is

probably related to the fact that the mouse body grows substantially over time while its head size

increases just slightly.
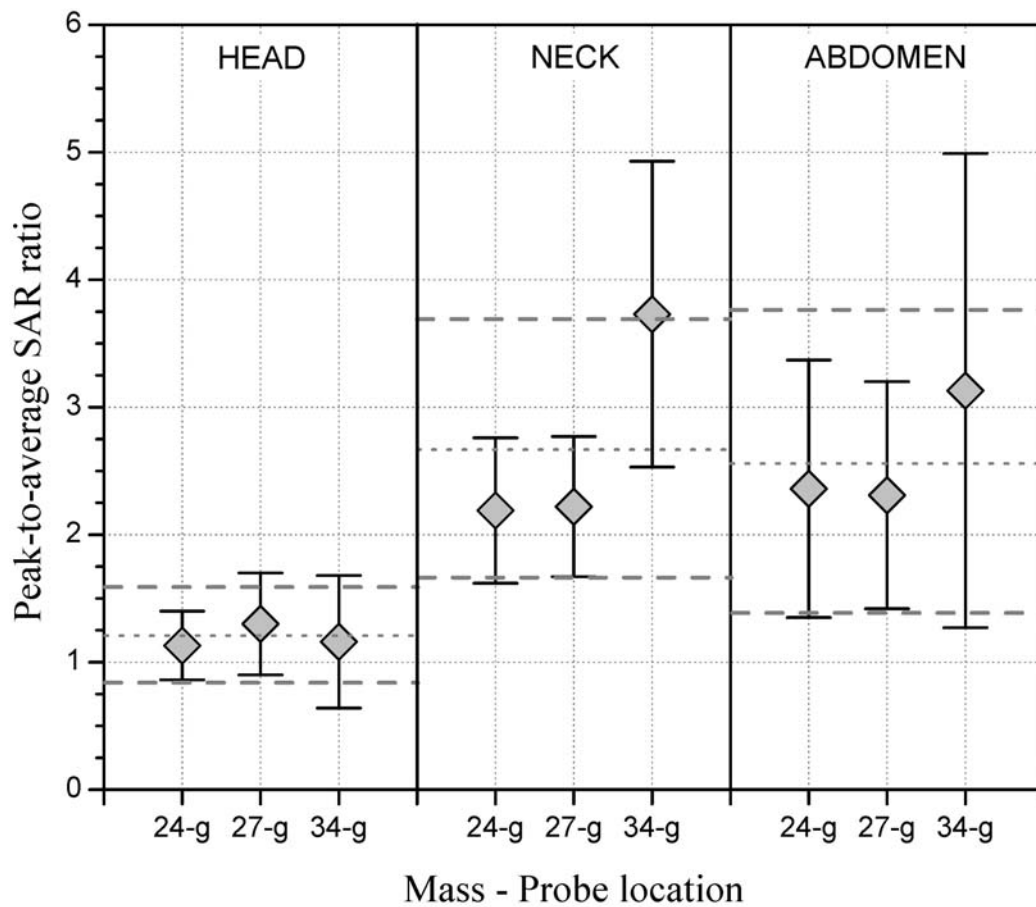
Fig. 19. Breakdown of the point-to-average SAR ratios by mass and location. Grand average

(dotted) and standard deviation (dashed) are indicated by location.

In some cases we observed discrepancies between the thermographic estimates and the corresponding thermometric measurements, especially when thermography produced a dominant hot spot in the head. For instance, the thermographic image in Figure 16a indicates that the highest SAR occurs in the head. However, the collective results displayed in Figure 19 indicate that the head SAR was consistently lower than in the other two hot-spots. The misleadingly high SAR level produced by IR imaging might be attributable to biological fluid (abundant in the head) spillage around the small head perimeter. Significantly less spillage was observed for the abdominal fluids.

DISCUSSION

The Ferris-Wheel dosimetry results can be used to estimate the RF exposure levels experienced by the mice over the two year exposure period in the IMVS bioassay. Such an analysis is intended to provide an estimate of the *collective* lifetime exposure accounting also for the daily random rotation around the wheel locations. Distribution curves of weight gain presented in Utteridge *et al.* (*1*) were employed to derive the collective mass values for the *wild-type* and the *transgenic* mice at four-month intervals that are reported in Table 5.

TABLE 5
Normalized SAR (±11%) versus collective mean weight reported in Utteridge *et al.* (*1*).

| Animal	Wild-type mice		Transgenic mice	
Age (months)	Mean weight (g)	SAR_{WBA} $(W\ kg^{-1}\ W^{-1})$	Mean weight (g)	SAR_{WBA} $(W\ kg^{-1}\ W^{-1})$
2	21.5	1.11	23.5	1.02
6	28.5	0.84	28.5	0.84
10	36.7	0.65	34.0	0.70
14	42.5	0.56	38.0	0.63
18	42.5	0.56	37.5	0.64
22	43.4	0.55	37.5	0.64
26	41.5	0.58	35.5	0.67
Averages	36.7	0.69	33.5	0.73

MOTOROLA LABS

The corresponding normalized SAR values are derived using Eq. 4, taking into account the uncertainty of the calorimetric SAR assessments performed on the mice ($\pm11\%$). Since the collective average lifetime mass is slightly larger than originally projected (30 g), it follows that the lifetime exposure experienced by the mice is somewhat less than anticipated. In particular, the mean lifetime exposure levels, reported in Table 6, are lower than the original targets by about 18% for the wild-type mice and about 10% for the transgenic mice.

TABLE 6
Mean lifetime WBA-SAR levels

Target SAR$_{WBA}$ (W kg^{-1} W^{-1})	Wild-type mice SAR$_{WBA}$ (W kg^{-1} W^{-1})	Transgenic mice SAR$_{WBA}$ (W kg^{-1} W^{-1})	Overall SAR$_{WBA}$ (W kg^{-1} W^{-1})
0.25	0.20	0.22	0.21
1.0	0.82	0.90	0.86
2.0	1.6	1.8	1.7
4.0	3.3	3.6	3.4

Collective WBA-SAR variation during the lifetime exposure. The distribution curves of weight gain in Utteridge *et al.* (*1*) show a more pronounced mass variation for the wild type mice, corresponding to ±1.5 dB peak-to-peak variation, compared with ±1.0 dB for the transgenic mice. As the IMVS Ferris-Wheel units were fed with constant power generators, the WBA-SAR was subject to the same lifetime variation. Excluding the first four months of exposure, when the mice grow very rapidly, the corresponding variations are ±0.9 dB and ±0.6 dB, respectively.

MOTOROLA LABS
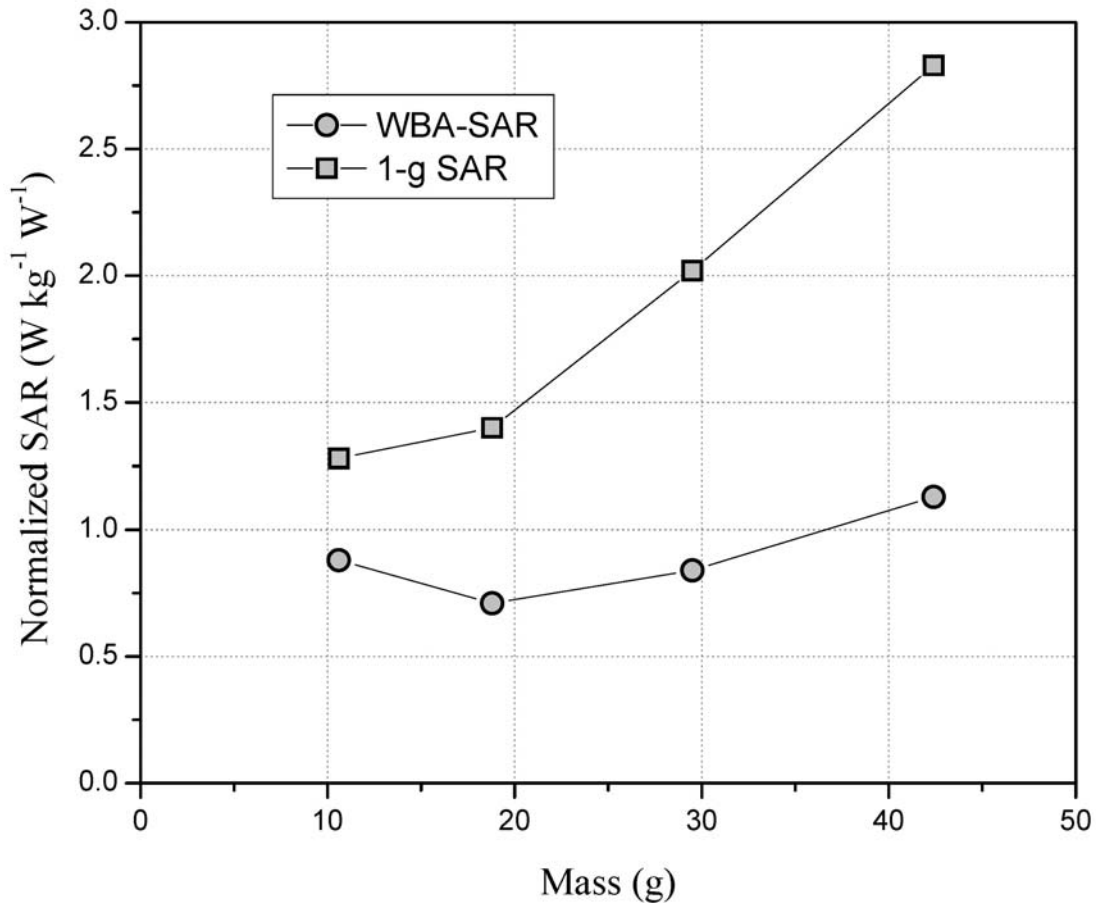
Fig. 20. Whole-body and 1-g average SAR dependence on dummy load mass computed using the computational Ferris-Wheel model featuring four different mass loads (Case #2).

An interesting observation is that the larger mice typically behave as better electromagnetic loads, in that their WBA-SAR is typically higher than for smaller mice in the asymmetric configurations analyzed computationally. However, as shown in Figure 20, such a behavior is not necessarily monotonous, at least for the WBA-SAR. Even though a specific investigation to verify its general character was not carried out, it is indeed important to note that the marked weight asymmetry simulated in Case #2 has not produced a correspondingly marked difference in SAR. Further studies on this aspect of the Ferris-Wheel behavior might be warranted to understand it fully.

Other dosimetry assessments that could be conveniently performed using numerical methods involve the analysis of the dependence of the individual and collective exposure uniformity on the Ferris-Wheel radius, its thickness, and the distance of the mice from its perimeter.

The results of the dosimetric study presented here indicate that the Ferris-Wheel exposure system fulfills the requirements set forth in its intended application at IMVS. We looked at the collective RF energy dose uniformity as the main quality criterion, as it enables reliable dose response assessments. Experimental and computational analyses indicated that the Ferris-Wheel behavior is robust with respect to asymmetries, degrading seriously only in some artificially exaggerated cases. Because of its exposure characteristics and the cost savings deriving from its energy and space efficiency (the fifteen IMVS units cost less than US$ 50,000 each including R&D and deployment costs, and fit easily in five mid-size rooms), the Ferris-Wheel concept has been adopted and further developed by other researchers to support a number of large scale bioassays commissioned by the European Union under the Fifth Framework Programme for Research (http://europa.eu.int/comm/research/fp5.html).

REFERENCES

1. T. D. Utteridge, V. Gebski, J. W. Finnie, B. Vernon-Roberts, and T. R. Kuchel. Long-term exposure of Eμ-Pim1 transgenic mice to 898.4 MHz microwaves does not increase lymphoma incidence. *Radiat. Res.* **158**, 357–364 (2002).

2. M. H. Repacholi, A. Basten, V. Gebski, D. Noonan, J. Finnie, and A. W. Harris. Lymphomas in Eμ-Pim1 transgenic mice exposed to pulsed 900 MHz electromagnetic fields. *Radiat. Res.* **147**, 631–640 (1997).

3. J. W. Finnie, P. C. Blumbergs, J. Manavis, T. D. Utteridge,V. Gebski, J. G. Swift, B. Vernon-Roberts, and T. R. Kuchel. Effect of Global System for Mobile Communication (GSM)-like RF fields on vascular permeability in mouse brain. *Pathology*. **33(3)**,338–340 (2001).

4. J. W. Finnie, P. C. Blumbergs, J. Manavis, T. D. Utteridge,V. Gebski, R. A. Davies, B. Vernon-Roberts, and T. R. Kuchel. Effect of long-term mobile communication microwave exposure on vascular permeability in mouse brain. *Pathology*. **34**, 344-347 (2002).

5. Q. Balzano, C. K. Chou, R. Cicchetti, A. Faraone, and R. Tay. An Efficient RF Exposure System with Precise SAR Estimation for In-Vivo Animal Studies at 900 MHz. *IEEE Trans. on Microwave Theory Tech*. **48**, 2040–2049 (2000).

6. T. D. Utteridge, V. Gebski, J. W. Finnie, B. Vernon-Roberts, T. R. Kuchel. Response to the Letters to the Editor sent by (1) Kundi, (2) Goldstein/Kheifets/van Deventer/Repacholi, and (3) Lerchl. *Radiat. Res.* **159**, 276–278 (2003)..

7. H. Bassen and T. Babij. Experimental techniques and instrumentation. In *Biological Effects and Medical Applications of Electromagnetic Energy* (O. P. Gandhi, Ed.). Prentice Hall, Englewood Cliffs, NJ, 1990.

8. C. K. Chou, H. Bassen, J. Osepchuk, Q. Balzano, R. Petersen, M. Meltz, R. Cleveland, J.C. Lin, and L. Heynick. Radio frequency electromagnetic exposure: Tutorial review on experimental dosimetry. *Bioelectromagnetics* **17**, 195–208 (1996).

9. C. K. Chou and A.W. Guy. Systems for exposing mice to 2450 MHz electromagnetic fields. *Bioelectromagnetics* **3**, 401–412 (1982).

10. C. K. Chou, A.W. Guy, J. A. McDougall, and H. Lai. Specific absorption rate in rats exposed to 2,450-MHz microwaves under seven exposure conditions. *Bioelectromagnetics*. **6**, 73-88 (1985).

11. C. K. Chou, A. W. Guy, and R. B. Johnson. SAR in rats exposed in 2450 MHz circularly polarized waveguide. *Bioelectromagnetics* **5**, 389–398 (1984).

12. A. W. Guy. Analysis of electromagnetic fields induced in biological tissues by thermographic studies on equivalent phantom models. *IEEE Trans. on Microwave Theory Tech*. **19**, 205–214 (1971).

13. K. A. Wickersheim and M. Sun. Fiberoptic thermometry and its applications. *J. Microwave Power* **22**, 85–94 (1987).

14. R. Bowman. A probe for measuring temperature in radio-frequency-heated material. *IEEE Trans. on Microwave Theory Tech*. **24**, 43–45 (1976).

15. K. W. Chan, C. K. Chou, J. A. Mc Dougall, and K. H. Luk. Perturbations due to the use of catheters with non-perturbing thermometry probes. *Int. J. Hyperthermia* **4**, 699–702 (1988).

16. J. S. Hart. Calorimetric determination of average body temperature of small mammals and its variation with environmental conditions. *Can J. Zool*. **29**, 224–233 (1951).

17. C. H. Durney, H. Massoudi, and M. F. Iskander. RF radiation dosimetry handbook. 4th Edition. Report SAM-TR-85-73, U.S. Air Force School of Aerospace Medicine (1984). (http://www.brooks.af.mil/AFRL/HED/hedr/reports/handbook/).

18. P. Bernardi, M. Cavagnaro, S. Pisa, and E. Piuzzi. Specific absorption rate and temperature elevation in a subject exposed in the far-field of radio-frequency sources operating in the 10-900-MHz range. *IEEE Trans. on Biomedical Engineering*. **50**, 295-304 (2003).

19. T. Weiland. A discretization method for the solution of Maxwell's equations for six component fields. *Electronics and Communications AEU*. **31(3)**, 116–120 (1977).

20. P. Russo and A. Faraone. Numerical analysis of the 'Ferris Wheel' mice exposure system using an efficient cylindrical FDTD scheme. *ACES J*. **16**, 181–189 (2001).